The EMBO Journal (2007) 26, 3868–3878 | © 2007 European Molecular Biology Organization | All Rights Reserved 0261-4189/07
www.embojournal.org

THE EMBO JOURNAL

Structural and functional insights into RAGE activation by multimeric S100B

Thorsten Ostendorp[1], Estelle Leclerc[2], Arnaud Galichet[2], Michael Koch[1], Nina Demling[3], Bernd Weigle[3], Claus W Heizmann[2], Peter MH Kroneck[1] and Günter Fritz[1,*]

[1]Fachbereich Biologie, Mathematisch-Naturwissenschaftliche Sektion, Universität Konstanz, Konstanz, Germany, [2]Department of Pediatrics, Division of Clinical Chemistry and Biochemistry, University of Zurich, Zürich, Switzerland and [3]Institute of Immunology, Medical Faculty Carl Gustav Carus, Technical University Dresden, Dresden, Germany

Nervous system development and plasticity require regulation of cell proliferation, survival, neurite outgrowth and synapse formation by specific extracellular factors. The EF-hand protein S100B is highly expressed in human brain. In the extracellular space, it promotes neurite extension and neuron survival via the receptor RAGE (receptor for advanced glycation end products). The X-ray structure of human Ca^{2+}-loaded S100B was determined at 1.9 Å resolution. The structure revealed an octameric architecture of four homodimeric units arranged as two tetramers in a tight array. The presence of multimeric forms in human brain extracts was confirmed by size-exclusion experiments. Recombinant tetrameric, hexameric and octameric S100B were purified from *Escherichia coli* and characterised. Binding studies show that tetrameric S100B binds RAGE with higher affinity than dimeric S100B. Analytical ultracentrifugation studies imply that S100B tetramer binds two RAGE molecules via the V-domain. In line with these experiments, S100B tetramer caused stronger activation of cell growth than S100B dimer and promoted cell survival. The structural and the binding data suggest that tetrameric S100B triggers RAGE activation by receptor dimerisation.

The EMBO Journal (2007) **26,** 3868–3878. doi:10.1038/sj.emboj.7601805; Published online 26 July 2007
Subject Categories: differentiation & death; structural biology
Keywords: RAGE; receptor dimerisation; S100B

Introduction

S100B is a member of the S100 protein family which represents the largest subgroup of EF-hand Ca^{2+}-binding proteins (Heizmann *et al*, 2002; Donato, 2003; Marenholz *et al*, 2004). The individual members of the S100 family show tissue- and cell type-specific expression patterns and regulate processes such as cell growth and motility, transcription and differentiation. S100 proteins except S100G (calbindin D_{9K}) mostly form homo- and heterodimers. Each subunit consists of two helix-loop-helix (EF-hand) motifs connected by a central linker or so-called hinge region. The C-terminal canonical EF-hand motif is composed of 12 amino acids, whereas the N-terminal S100-specific EF-hand comprises 14 residues. The S100 proteins undergo a conformational change upon Ca^{2+} binding, which leads to the exposure of a protein–protein interaction site (Ikura and Ames, 2006).

S100B is mainly synthesised by astrocytes in human brain and modulates long-term synaptic plasticity (Nishiyama *et al*, 2002). Intracellularly, S100B modulates microtubule assembly and regulates the cell cycle by interacting with transcription factors such as p53. Upon changes in intracellular Zn^{2+} and Ca^{2+} concentrations, S100B is secreted from glia cells to the extracellular space, where it exhibits cytokine-like functions (Davey *et al*, 2001). The action of S100B is strongly dependent on its extracellular concentration. At nanomolar level, S100B is neuroprotective, whereas it promotes apoptosis at micromolar concentration (Huttunen *et al*, 2000; Businaro *et al*, 2006). Such high extracellular levels are detected after traumatic brain injury or in neurodegenerative disorders like Down's Syndrome, Alzheimer disease or encephalomyelitis (Griffin *et al*, 1998; Mrak and Griffin, 2001). Both trophic and toxic effects of extracellular S100B are mediated in the brain by the receptor RAGE (receptor for advanced glycation end products) (Hofmann *et al*, 1999), which was initially described as a receptor for glucose-modified proteins, involved in the development of chronic inflammations in diabetes patients (Neeper *et al*, 1992).

RAGE is a member of the immunoglobulin (Ig) superfamily of cell-surface receptors and shares homology with neuronal cell adhesion molecules like NCAM or axonin (Freigang *et al*, 2000; Soroka *et al*, 2003). RAGE consists of an extracellular moiety, a single transmembrane spanning helix and a short cytosolic domain which is required for signal transduction. The extracellular moiety includes one N-terminal V-type and two C-type Ig domains. Increased RAGE expression is observed in human diseases including diabetes, Alzheimer disease and inflammations (Ramasamy *et al*, 2005). The levels of RAGE rise upon stimulation through extracellular ligands, resulting in an increasing cellular response and establishment of a chronic inflammation. To disrupt this cycle, detailed knowledge of the nature of the ligand–receptor interaction is required. Although comprehensive structural information on S100B is available, the known structures reflect only the intracellular state of S100B. Extracellularly, S100B can form disulphide bonds required for its neurite extension activity (Selinfreund *et al*, 1991; Kiryushko *et al*, 2006), but not for the pro-inflammatory activity of S100B (Koppal *et al*, 2001). The presence of disulphide bonds suggests the formation of covalently linked multimers, but leaves the state of pro-inflammatory acting S100B questionable. Here, we report the detection of noncovalent S100B

*Corresponding author. Fachbereich Biologie, Mathematisch-Naturwissenschaftliche Sektion, Universität Konstanz, Universitätsstrasse 10, Konstanz 78457, Germany.
Tel.: +49 7531 88 3205; Fax: +49 7531 88 2966;
E-mail: guenter.fritz@uni-konstanz.de

Received: 13 February 2007; accepted: 29 June 2007; published online: 26 July 2007

multimers in human brain. Stable S100B multimers were purified from *Escherichia coli* and bound with high affinity to the extracellular domain of RAGE (sRAGE). The crystal structure of human S100B revealed a noncovalent octameric assembly consisting of two tetramers. On the basis of these structural data, binding studies and *in silico* docking calculations, we propose that tetrameric S100B activates RAGE through receptor dimerisation.

Results

S100B multimers in human brain

The presence of multimeric S100B in human brain extract was demonstrated by size-exclusion chromatography (SEC). The elution profile of S100B from SEC was monitored by an ELISA test specific for S100B. In the presence of Ca^{2+}, S100B elutes in three superimposing peaks corresponding to tetramer, hexamer and octamer, whereas in the presence of EDTA, S100B elutes in two major peaks corresponding to tetramer and dimer (Figure 1B). The high molecular mass peaks of S100B, in the presence of Ca^{2+}, might represent higher multimers such as hexamer and octamer, but could also represent complexes of Ca^{2+}-loaded S100B dimer or S100B tetramer with target proteins. However, calculating the molecular masses of complexes of known target proteins with S100B dimer reveals that most complexes are much larger than the observed peaks (Supplementary Figure I). We therefore conclude that the observed peaks mainly represent the larger multimers such as hexamer and octamer of S100B.

In the presence of EDTA, which abolishes S100B–target protein interactions, about 50% of the protein elutes as tetramer and 50% as dimer (Figure 1A). The elution profiles document the presence of oligomers of S100B in the brain and reveal that multimers represent a large portion of S100B in human brain.

Biochemical characterisation of human recombinant multimeric S100B

Purification of recombinant human S100B from *E. coli* yields dimeric, tetrameric, hexameric and octameric S100B (Ostendorp *et al*, 2005). These multimers were stable and isolated multimers eluted as one major peak from SEC (Figure 1C). No equilibrium between the different S100B species was observed. Upon freezing and thawing, octameric and hexameric S100B partially dissociated into tetramers and dimers. In contrast, tetrameric S100B was stable and did not dissociate further into dimers. The molecular masses of the different multimeric species were judged from a calibration of the column with proteins of known size. The mass of the isolated S100B species was further analysed by analytical ultracentrifugation (Figure 1D). Analysis of the sedimentation behaviour revealed masses of 21 kDa for dimeric, 41 kDa for tetrameric, 61 kDa for hexameric and 82 kDa for octameric S100B, which are in good agreement with the calculated masses (dimer 21.4 kDa, tetramer 42.8 kDa, hexamer 63.2 kDa and octamer 85.6 kDa).

The Ca^{2+}-induced conformational change of dimeric S100B has been well characterised by NMR and X-ray crystal-

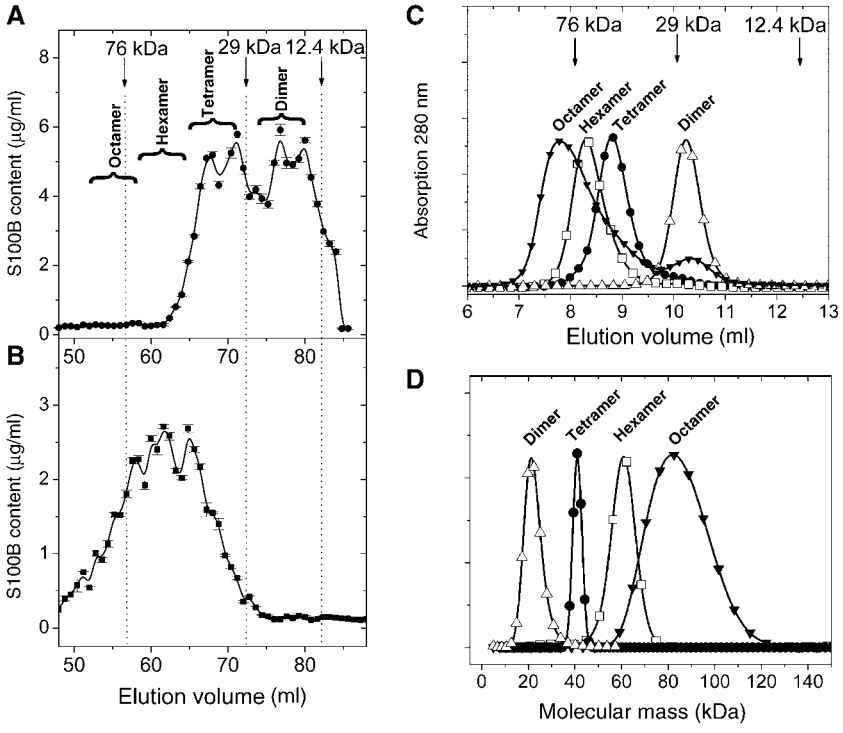

Figure 1 Detection and molecular mass analysis of S100B multimeric species. Human brain extracts were analysed by SEC. (**A**) Elution profile of S100B from human brain extract in the presence of EDTA. (**B**) Elution profile of S100B in human brain extracts in the presence of Ca^{2+}. The elution volumes of standards (cytochrome *c* 12.4 kDa, carboanhydrase 29 kDa, conalbumin 76 kDa) and the elution volumes of isolated recombinant S100B species from the same column are indicated. (**C**) Elution profiles of isolated recombinant S100B species (dimer △; tetramer ●, hexamer □, octamer ▼) from analytical SEC. The elution volumes of standards are indicated. (**D**) Analysis of the isolated S100B multimers by analytical ultracentrifugation. The fits for molecular mass distribution for S100B dimer (–△–), tetramer (–●–), hexamer (–□–) and octamer (–▼–) samples are shown.

lographic studies (Kilby *et al*, 1996; Matsumura *et al*, 1998; Drohat *et al*, 1998a, 1999). These studies showed that dimeric S100B undergoes a conformational change upon Ca^{2+} binding, leading to the exposure of a hydrophobic patch at the surface of the molecule. To test whether the isolated multimers undergo, like dimeric S100B, a Ca^{2+}-dependent conformational change, the different species were bound in the presence of Ca^{2+} to hydrophobic phenyl–Sepharose matrix and eluted from the matrix with EDTA. Subsequent analysis of the eluting protein by analytical SEC showed that the multimers did not dissociate on the phenyl–Sepharose column. Thus, the different multimeric S100B species are fully functional as Ca^{2+}-sensor proteins like the S100B dimer.

The secondary structures of the dimeric, tetrameric and octameric S100B were analysed by far UV-CD spectroscopy. The CD spectra of the different species were virtually identical (Supplementary Figure IVA) and showed that all S100B species were correctly and presumably identically folded. The content of α-helix as determined by CD spectroscopy was 64% and fits very well the X-ray structural data with 63% α-helix as determined by DSSP (Kabsch and Sander, 1983). These results demonstrate that the S100B multimers are fully folded and functional.

Previous studies revealed that a disulphide linked form of S100B is required for its neurotrophic activity (Selinfreund *et al*, 1991), but not for the induction of an inflammatory response in glia cells (Koppal *et al*, 2001). The S100B multimers studied here were not bridged by intermolecular disulphide bonds as shown by SDS–PAGE under nonreducing conditions (Supplementary Figure IVB). Furthermore, we expressed and purified a Cys→Ser mutant of S100B, which gave the same distribution of dimeric, tetrameric, hexameric and octameric S100B in SEC experiments. This demonstrates that neither the formation of the multimers nor their stability is dependent on disulphide bridges. The X-ray structure reported here confirms our data from biochemical studies.

Tetrameric S100B promotes stronger cellular growth and survival of HeLa cells

S100B is released by cells into the intracellular space and can directly affect cells (Davey *et al*, 2001). To examine the role of S100B multimerisation in cellular functions, we treated HeLa cells with both S100B dimers and tetramers. We had observed previously that hexameric and octameric S100B partially dissociated, respectively, into tetramer and dimer upon freezing and thawing. Therefore, we tested the stability of the different S100B species in cell culture media at 37°C before the cell activation assays. The different species of S100B were analysed by SEC on a Superdex 75 column. After 24 h, octameric and hexameric S100B were dissociated into tetramers and dimers and only ca. 20% of the original amount of the largest species was still present. In contrast, tetrameric S100B remained intact up to 12 h and after 24 h 80% of the original tetramer was still observed under the same conditions. S100B dimer did not form any larger oligomers even after 48 h at 37°C in cell culture medium. Therefore, we used only dimeric and tetrameric S100B for cell activation assays. To clearly resolve the effect of dimeric and tetrameric S100B, we used the same mass concentration of protein (100 μg/ml), that is, the molar concentration of S100 tetramer (2.35 μM) was just half of the concentration of S100B dimer (4.7 μM) in the assays. Nevertheless, exogenous tetrameric S100B

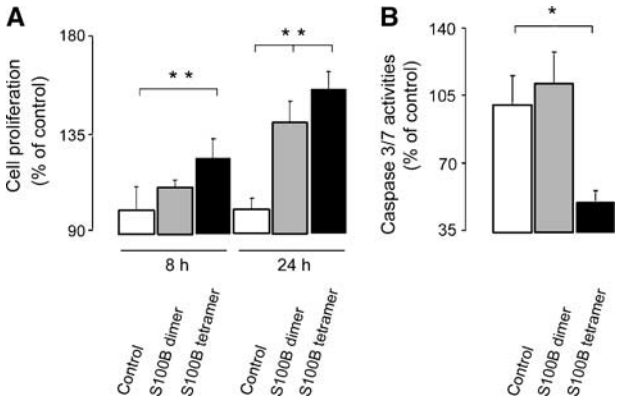

Figure 2 S100B tetramers activate HeLa cells differently than S100B dimers. (**A**) Effect of S100B dimers (100 μg/ml, 4.7 μM) and tetramers (100 μg/ml, 2.35 μM) on cell proliferation was estimated after 8 and 24 h treatment by MTT assay ($n=8$). (**B**) Effector caspase 3 and 7 activities were similarly monitored after 8-h treatment with PBS alone or S100B species ($n=4$). All data are expressed as means ± s.d. Statistical analysis was performed using one-way analysis of variance, followed by Student's *t*-test. Significance was considered as $P \leqslant 0.0001$ (**) or $P \leqslant 0.001$ (*) versus the control group.

increased cell proliferation already after 8 h, whereas cells treated with the dimeric form of the protein only showed increased proliferation after 24 h (Figure 2A). Similarly, S100B tetramers-treated cells had decreased caspase 3/7 activities compared with control or S100B dimers-treated cells (Figure 2B). These results corroborate that the multimerisation state of S100B strongly affects its function. The stronger activation of cell proliferation and cell survival by S100B tetramer, although the molar concentration was only half of that of the S100B dimer, can be readily explained by stronger binding of S100B tetramer to RAGE as observed in surface plasmon resonance (SPR) experiments (see below).

Crystal structure of S100B

Overall structure. Human recombinant S100B in the Ca^{2+}-loaded state was successfully crystallised (Ostendorp *et al*, 2005) and the X-ray structure was refined to 1.9 Å resolution. The crystals grew from protein precipitates to a final size of $0.2 \times 0.4 \times 0.4$ mm. The space group is $P2_1$ with unit cell parameters, $a=63.4$ Å, $b=81.6$ Å, $c=71.5$ Å, $\alpha=\gamma=90°$, $\beta=107°$. The structure is well defined by the electron density except four side chains located at the protein surface and two residues in the C-terminal regions of the S100B subunits could not be resolved. The final model contains 728 amino-acid residues, 18 Ca^{2+} ions, one PEG400 and 713 water molecules, and converged to a R_{cryst} of 17.4% and R_{free} of 24.0% using Refmac (Murshudov *et al*, 1997) for final refinement (Table I). The asymmetric unit contains four S100B dimers, which are related by an approximate noncrystallographic 222 symmetry (Figure 3A). This approximate 222 symmetry is very close to 180° for the pair of dimers AB–CD (179°) and EF–GH (178°), but exhibits lower symmetry for the AB–GH (174°) and CD–EF (172°) pairs, respectively (Supplementary Figure II). This difference in the pairings is also observed in the r.m.s.d.s, which are 0.91 and 0.59 Å for the AB–CD and EF–GH pairs, respectively, whereas the

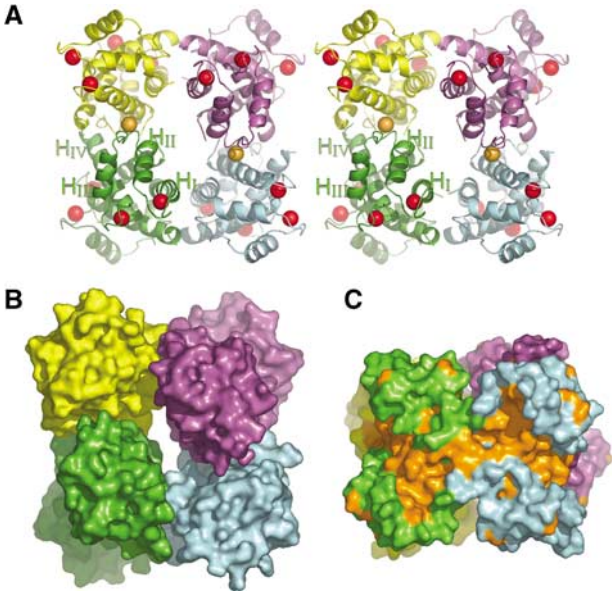

Figure 3 Overall structure of the S100B octamer. (**A**) Arrangement of eight S100B subunits (A–H) in the octamer. The view is down one noncrystallographic two-fold axis. The second noncrystallographic two-fold axis is vertical, and the second noncrystallographic two-fold axis is horizontal. Subunits AB are shown in green, CD in cyan, EF in magenta and GH in yellow. The Ca^{2+} ions are shown as spheres. Sixteen Ca^{2+} ions located in the EF-hand are shown in red and two Ca^{2+} ions bound at the subunit interface are shown in orange. (**B**) Surface representation of the octamer showing the tight assembly of the subunits. (**C**) Hydrophobic surface of S100B octamer. The side view of S100B shows the large hydrophobic surface (orange) formed by two adjacent S100B dimeric units (AB and CD) of the octamer.

Table I Data collection and refinement statistics

Wavelength (Å)	1.54
Resolution limit (Å)	30–1.90 (2.0–1.9)[a]
I/σ	15.9 (4.0)[a]
Space group, Unit cell (Å)	$P2_1$; $a=63.4$, $b=81.6$, $c=71.5$, $\alpha=\gamma=90^\circ$, $\beta=107^\circ$
Completeness (%)	98.9 (94.1)
Multiplicity	3.6
$R_{mrged\text{-}F}$ (%)[b]	7.8 (31.5)[a]
Resolution range	30–1.9
R_{cryst} (%)[c]	17.4 (19.9)[a]
R_{free} (%)[d]	24.0 (25.5)[a]
RMS bond length (Å)	0.017
RMS bond angles (deg)	1.6

[a]The numbers in parentheses are the statistics for the highest resolution shell.
[b]$R_{mrgd\text{-}F}$ (%) $= \Sigma\ (|AI_{h,P}-AI_{h,Q}|)/(0.5*\Sigma AI_{h,P}+AI_{h,Q})$.
[c]$R_{cryst}=\Sigma_{hkl}(|F(obs)|-|F(calc)|)/\Sigma_{hkl}|F(obs)|$.
[d]$R_{free}=\Sigma_{hkl}(|F(obs)|-|F(calc)|)/\Sigma_{hkl}|F(obs)|$, where 5% of the observed reflections are not used for refinement.

AB–GH and CD–EF pairs exhibit in each case higher r.m.s.d.s of 1.01 and 0.86 Å. These differences suggest that the dimers AB and CD form one tetramer, whereas the other tetramer is formed by the dimers of chains EF and GH. This assignment of two dimers to a tetramer is corroborated by the analysis of the interdimer interfaces, which show that for example, the dimers AB and CD cover a larger surface (1540 $Å^2$) than the dimers AB and GH (1230 $Å^2$).

The S100B octamer has a donut-like shape, with a diameter of 82 Å, containing a central cavity with an approximate diameter of 10 Å (Figure 3B). The four dimers in the assembly are very similar to the so far determined 3D structures of S100B, like for example, the crystal structure of bovine S100B (pdb code 1MHO) (Matsumura *et al*, 1998), as illustrated by an r.m.s.d. of 1.0 Å for 174 Cα positions. Each subunit in the octamer consists of two pairs of EF-hands connected by a flexible linker region. The Ca^{2+} ions in the EF-hands of the subunits are well defined by the electron density and are coordinated by the sidechains of Asp and Glu residues and by backbone carbonyl oxygen atoms. The X-ray structure of human S100B revealed structural changes induced by Ca^{2+} binding similar to the structures of Ca^{2+}-loaded rat and bovine S100B (Matsumura *et al*, 1998; Drohat *et al*, 1998a). Comparison with structures of Ca^{2+}-free S100B from rat (Drohat *et al*, 1999) reveals that Ca^{2+} binding induces a rather small conformational change in the N-terminal S100-specific EF-hand, but a large change in the canonical C-terminal EF-hand. Helix H_{III} moves by about 90°, changing the orientation of helix H_{III} towards helix H_{IV} from an antiparallel to a perpendicular orientation. The N-terminal helices (H_I) of the eight subunits outline the central cavity of the octameric structure (Figure 3A and B), whereas helices H_{II} reside at the top and the bottom of the octameric molecule. The C-terminal EF-hands of all subunits encompassing helices H_{III} and H_{IV} are exposed to the solvent at the side of the octameric structure. This arrangement leads to an accumulation of hydrophobic surface areas, which combine to a large putative target-binding site (Figure 3C). To get an idea of the structural changes in the tetramer induced by Ca^{2+} binding, we built a model of Ca^{2+}-free S100B tetramer using the structure of rat S100B in the Ca^{2+}-free form (Drohat *et al*, 1999). In the model, the conformation of helix H_{IV} had to be slightly adjusted to form the interdimer contact of the tetramer. Surface analysis of the Ca^{2+}-free tetramer model showed that the large hydrophobic area observed in the structure of Ca^{2+}-loaded S100B tetramer (Figure 3C) was absent (data not shown). As expected, in the model of Ca^{2+}-free tetramer, a part of the hydrophobic area was covered by helices H_{III} of the C-terminal EF-hands. The hydrophobic patch observed in the centre between the two dimers was masked in the Ca^{2+}-free form by residues of the linker regions. Thus, conformational changes of helices H_{III} and of the linker regions lead to the exposure of hydrophobic patches, which combine to the large area observed in the structure. Remarkably, in a tetrameric or octameric S100B, two target protein interaction sites get in close proximity on one face of the molecule. Binding of tetrameric or octameric S100B will possibly approach target proteins in such a way that intermolecular interactions between the target molecules become likely. In contrast, the two target interaction sites in dimeric S100B reside on opposite sides of the molecule (Rustandi *et al*, 2000; Inman *et al*, 2002; Bhattacharya *et al*, 2003; McClintock and Shaw, 2003), making intermolecular interactions between the bound target molecules unlikely.

Intermolecular interactions of the S100B subunits in the octamer

The size of the buried area at the interface between two dimers (subunits A–B, C–D) forming a tetramer (A–B–C–D) is 1540 $Å^2$ which is in the typical range (1600 ± 400 $Å^2$) for

protein–protein complexes (Lo Conte *et al*, 1999). The residues at the interface between dimers AB and CD, as well as between dimers EF and GH provide a number of hydrophobic contacts as well as five hydrogen bonds (Figure 4A–C). Assembly of the two tetramers ABCD and EFGH to the octamer buries a total surface area of ca. 2500 Å^2. The interface is formed by a number of hydrophobic and polar interactions: for example, the hydrophobic residues Ile11 of subunit D and Cys84, Phe87 and Phe88 of subunit C shape a pocket which embeds the residues Phe87 and Phe88 of subunit E. At the interface between the two tetramers, two additional binding sites for Ca^{2+} were identified in the electron density difference maps. The geometry and bond distances as analysed by the program WASP (Nayal and Di Cera, 1996) and the electron density are in agreement with Ca^{2+} bound to the sites. Each Ca^{2+} ion is coordinated by residues from two different subunits and water molecules. Ser41 and Leu44 from one subunit (B or E) provide backbone carbonyl oxygens, whereas Asp12 from subunit H or D provides the sidechain for coordination of the Ca^{2+}. The coordinated water molecules are stabilised by a hydrogen bond network around the binding site (Figure 5). Such additional Ca^{2+} ions at the interface of subunits were also observed in the hexameric structure of S100A12 (Moroz *et al*, 2002). The contact sites between the dimeric units in the S100B octamer structure show a rather high geometric surface complementarity, which most likely contribute to the stability of the octameric complex. Shape complementarity can be quantitated by defining a shape correlation statistic (*Sc*) that measures the degree of geometric match between two juxta-posed surfaces (Lawrence and Colman, 1993). Interfaces with perfect fits have $Sc = 1$, whereas interfaces that are topographically uncorrelated have *Sc* values close to zero. The high shape correlation statistics (*Sc* values) of 0.68 for the interface formed by two dimers (AB + CD) are in the same range like those for S100B target peptide complexes (Rustandi *et al*, 2000; Inman *et al*, 2002; Bhattacharya *et al*, 2003; McClintock and Shaw, 2003), which gave an average value of 0.62 ± 0.09. The *Sc* value of 0.76 for the interface between two S100B tetramers (ABCD + EFGH) is even higher than in antibody/antigen complexes which exhibit typical values of 0.64–0.68 (Lawrence and Colman, 1993).

To validate the interdimer and intertetramer interfaces, we compared the sequences of S100B from nine species. The residues involved in the interdimer and intertetramer contacts are all strictly conserved in S100B. Remarkably, S100B exhibits the highest grade of conservation among all S100 proteins with 96% identity over 91 residues (Supplementary Figure IIIA).

Furthermore, we constructed two S100B variants where Asp12 or Phe87/Phe88 were exchanged to Ala. Both variants were isolated by the same procedure as S100B wild type. SEC showed that recombinant S100B-D12A and S100B-F87AF88A form mainly dimer (87%/81%) and much less tetramer (9%/10%) or hexamer (3%/9%) compared to recombinant S100B wild type (61 ± 8 dimer, 25 ± 7 tetramer, 11 ± 3 hexamer, 3 ± 1.4 octamer; $n = 4$) (data are summarised in Supplementary Table I). Octameric S100B was not detected for both variants. These results strongly support that the crystallographically observed interfaces reflect the situation in solution and are not an artefact of crystal packing.

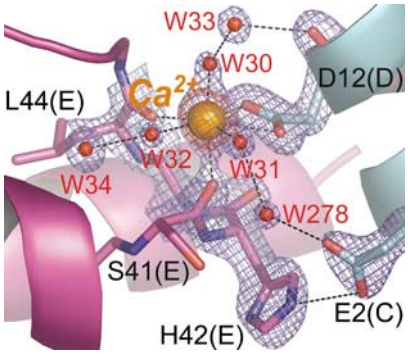

Figure 5 Intersubunit Ca^{2+}-binding site. View of the CD–EF intersubunit Ca^{2+}-binding site. Ca^{2+} coordination and hydrogen bonds are indicated by dashed lines. Ca^{2+} to oxygen distances are in the range of 2.2–2.6 Å. The Ca^{2+} (orange sphere) is coordinated in a distorted octahedral manner by the side chain of Asp 12D, backbone carbonyls from Ser41E and Leu44E and the water molecules W30, W31 and W32 (red spheres). A 2fo−fc electron density (blue) is shown countered at 1.5 σ and a fo-fc map, where the Ca^{2+} was omitted is countered at 7.0 σ (red).

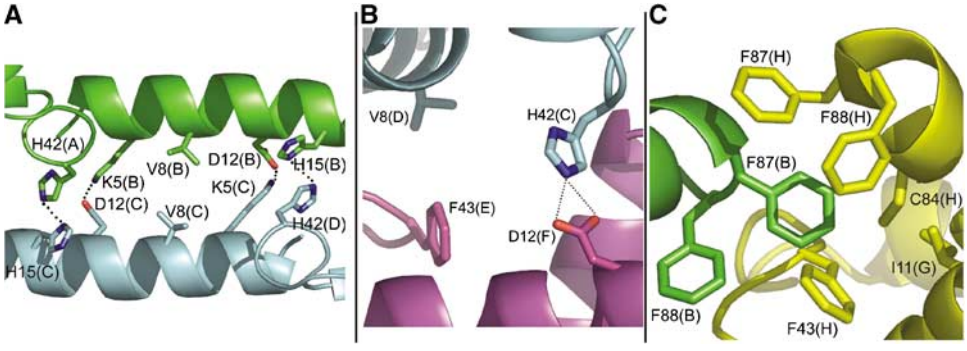

Figure 4 Interactions of subunits in S100B octamer. (**A**) Subunit contact formed by two antiparallel oriented helices of subunits A, B, C and D. Hydrogen bounds and salt bridges are formed between Asp12B and Lys5C, Asp12C and Lys5B, His 15B and His42D, and between His42A and His15C. Additional hydrophobic contacts are formed by Val8 of subunits B and C. (**B**) Interactions between subunits C, D, E and F. There are hydrophobic contacts between Val8D and Phe43E, as well as ionic interactions between by His42C and Asp12F. (**C**) Hydrophobic interactions formed by C-terminal residues. The subunits AB–GH are linked by a hydrophobic knot formed by residues Phe87B and Phe88B and Ile11G, Cys84H, Phe87H and Phe88H.

S100B binding to sRAGE

The binding modes of S100B to intracellular target proteins have been characterised in great detail. Upon Ca^{2+} binding, the structure opens and exposes a protein–protein interaction site. The interaction site of S100B provides hydrophobic and polar residues which are required for high-affinity binding of p53 (Rustandi *et al*, 2000), CapZ (Inman *et al*, 2002; McClintock and Shaw, 2003) or Ndr-kinase (Bhattacharya *et al*, 2003). The extracellular S100B cytokine-like function requires specific binding with receptors such as RAGE. The nature and properties of RAGE–S100B binding, as well as the influence of S100B oligomerisation, have not been characterised so far. We investigated the binding of the different S100B species to the sRAGE by ELISA and dot blot overlay techniques. In both assays, we observed high-affinity binding of different S100B species to sRAGE from HEK293 cells or from *Pichia pastoris* (Supplementary Figure V).

Kinetic analysis of S100B–sRAGE interaction

The binding of S100B to the sRAGE was further studied by SPR. As octameric and hexameric S100B showed some dissociation after freezing/thawing cycles, the SPR measurements were carried out with dimeric and tetrameric S100B. Both proteins were stable under the experimental conditions as shown by analytical SEC and ultracentrifugation (Figure 1). Binding studies were performed using recombinant human sRAGE fused at the C terminus to the glutathione-S-transferase (GST) protein. Immobilisation of this fusion protein using an antibody against GST resulted in unidirectional orientation of sRAGE on the sensor chip, mimicking the orientation of RAGE on the cell surface. The experimental data clearly showed binding of dimeric and tetrameric S100B to sRAGE. The binding was strictly Ca^{2+}-dependent. This implies that structural features, which are involved in intracellular signalling via protein–protein interactions, are also utilised in extracellular signalling to bind RAGE.

Analysis of the data with dimeric S100B revealed a moderate affinity to sRAGE ($K_d = 8.3\,\mu M$) (Figure 6A). The data fitted well with a simple model of interaction, where one S100B dimer interacts with one immobilised sRAGE molecule (equation 1).

$$S100B_{dimer} + sRAGE \underset{k_{off}1}{\overset{k_{on}1}{\rightleftharpoons}} S100B_{dimer} - sRAGE \qquad (1)$$

However, the analysis of the data for tetrameric S100B showed that their binding curves required a more complex model (Equation 2). Two different forms of sRAGE (sRAGE and sRAGE*) had to be assumed, which gave a much better fit of the data.

$$S100B_{tetramer} + sRAGE \underset{k_{off}1}{\overset{k_{on}1}{\rightleftharpoons}} S100B_{tetramer} - sRAGE \qquad (2)$$

$$S100B_{tetramer} + sRAGE^* \underset{k_{off}2}{\overset{k_{on}2}{\rightleftharpoons}} S100B_{tetramer} - sRAGE^*$$

The SPR data document clearly that tetrameric S100B bound sRAGE with higher affinity than dimeric S100B (Figure 6A and B). One population of tetrameric S100B (66%) bound to sRAGE with an eightfold higher affinity ($K_{d1} = 1.1\,\mu M$) compared with dimeric S100B. A second population of tetrameric S100B (34%) bound sRAGE with about

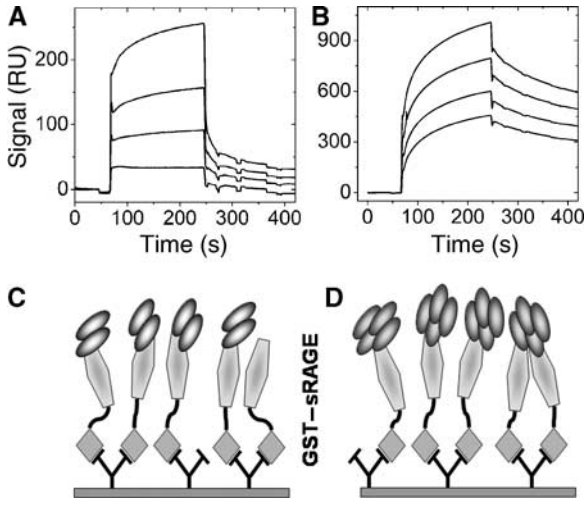

Figure 6 SPR analysis of S100B-RAGE interaction. (**A**) S100B dimer binds to captured GST-sRAGE displaying a $K_{d1} = 8.3\,\mu M$. (**B**) Binding or S100B tetramer to GST–sRAGE. Fitting of the curves with the parallel reaction model revealed two different binding modes with $K_{d1} = 1.1\,\mu M$ and $K_{d2} = 0.04\,\mu M$. (**C**, **D**) Graphical illustration of the interpretation of the binding data. GST–sRAGE is immobilised unidirectional and the sRAGE moiety is connected by a flexible linker facilitating lateral motion of the sRAGE moiety. This type of immobilisation allows dimerisation of the sRAGE moiety resulting in higher affinities for S100B tetramer.

500-fold higher affinity ($K_{d2} = 42\,nM$) than dimeric S100B. Comparison of the kinetic parameters revealed that, in particular, the dissociation of tetrameric S100B is 15-fold slower than for dimeric S100B (Table II). Slower dissociation of the ligand from the receptor results in longer activation of the receptor-dependent signal pathway, which in turn generates a stronger cellular response. Thus, the SPR data are in full agreement with the results from the cell activation assays (Figure 2), which revealed a stronger activation of cell proliferation and survival of HeLa cells by tetrameric S100B. The observed two populations of S100B tetramer in SPR measurements indicate that the multimeric protein can bind in two different modes to RAGE. On the other hand, our spectroscopic and structural data show that both the immobilised sRAGE and tetrameric S100B are homogenous. We suggest that the two binding populations represent binding to monomeric and dimeric forms of the immobilised receptor. As the GST–sRAGE fusion proteins are captured via an anti-GST IgG antibody to the sensor chip, two GST–sRAGE molecules can be captured with one IgG at the same time. Moreover, the flexible linker between GST and sRAGE allows lateral motion of the sRAGE moiety. The dimerisation of sRAGE could be triggered by the binding of tetrameric S100B to sRAGE. It is also possible, that some receptor dimer is already present on the sensor chip that is specifically recognised by tetrameric S100B. Indeed, the crystal structure presented here shows that the protein–protein interaction sites of two S100B molecules are located side by side at the same face of tetrameric S100B. We suggest that the high-affinity interaction site occurs between tetrameric S100B and the dimeric sRAGE.

Stoichiometry of S100B and V-domain complexes

To investigate the proposed multimerisation, we expressed and purified the V-domain of human RAGE and performed analytical ultracentrifugation runs of S100B dimer and tetra-

Table II Binding constants from surface plasmon analysis of S100B–RAGE interaction

S100B	$k_{on\ 1}$ ($M^{-1}\,s^{-1}$)	$k_{off\ 1}$ (s^{-1})	$k_{on\ 2}$ ($M^{-1}\,s^{-1}$)	$k_{off\ 2}$ (s^{-1})	$K_{d\ 1}$ (M)	$K_{d\ 2}$ (M)	Species 1 (%)	Species 2 (%)
Dimer	1.59×10^{3}	1.32×10^{-2}	—	—	8.3×10^{-6}	—	100	—
Tetramer	1.73×10^{3}	1.90×10^{-3}	5.0×10^{4}	2.1×10^{-3}	1.1×10^{-6}	4.2×10^{-8}	66	34

mer with V-domain. We showed in a recent study that S100B binds with high affinity ($K_d = 0.5\,\mu M$) to V-domain of RAGE (Dattilo *et al*, 2007). At the chosen concentrations of 25–50 μM for S100B and V-domain in the analytical ultracentrifugation experiments, the formation of a complex is favoured. Mixing of the proteins at pH 7.5 at temperatures below 20°C resulted in precipitation indicating the formation of a complex with decreased solubility. Therefore, analytical ultracentrifugation runs were performed at 28°C. Covalent linkage between S100B and V-domain was ruled out by analysis on nonreducing SDS–PAGE and by control experiments using the S100B-C68S-C84S variant. Analytical ultracentrifugation revealed that V-domain exists predominantly as monomer (71%), but a dimeric form (29%) was observed as well (Figure 7A, upper trace). A mixture of equimolar amounts of dimeric S100B with V-domain formed a complex with a size of 36 kDa (Figure 7A, lower trace), which is in reasonable agreement with the calculated mass of 33.9 kDa of a complex formed by one S100B dimer and one molecule of V-domain. No residual S100B dimer or V-domain was observed. Analysis of mixtures containing the double amount of V-domain per S100B dimer showed that two major species with a mass of 13 and 54 kDa have formed (Figure 7A, middle trace). The 13 kDa species represents most likely residual V-domain (calculated mass 12.5 kDa), which was not bound by S100B dimer. The 54 kDa species must contain S100B and V-domain. A complex of two S100B dimers and one V-domain (calculated mass 54.9 kDa) would fit the mass. Complex formation was also observed for S100B tetramer and RAGE V-domain. Mixing S100B tetramer and V-domain in a 1:2 ratio resulted in the formation of a complex of 67 kDa (Figure 7B, lower trace), which is in agreement with one S100B tetramer bound to two V-domains (calculated mass 67.8 kDa). Only minor residuals with low molecular mass were observed at a 1:2 ratio between S100B tetramer and V-domain. However, mixing a 1:4 ratio of S100B tetramer with V-domain (1 V-domain per 1 S100B subunit) gave no larger complex. Again the 67-kDa complex and a large amount of residual V-domain was observed, which was not bound by S100B tetramer (Figure 7B, middle trace). The data substantiate the conclusion from the SPR data and indicate that S100B tetramer might trigger RAGE dimerisation by binding to the V-domain of two receptor molecules.

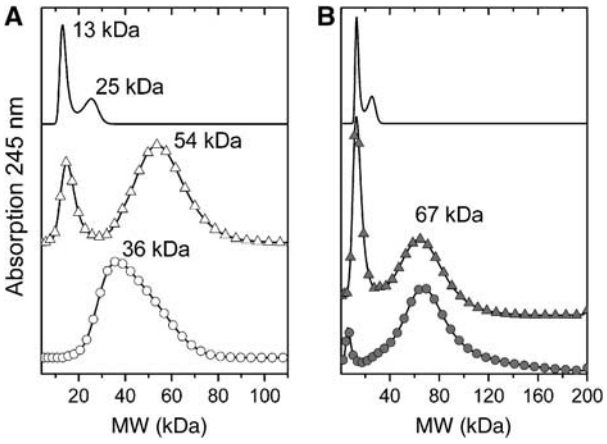

Figure 7 Complex formation a of S100B dimer and tetramer with V-domain of RAGE. The traces show the fits for molecular mass distribution from analytical ultracentrifugation (**A**) The upper trace (—) shows that V-domain occurs as monomer (74%) as well as dimer (26%). The middle trace (–△–) shows the S100B dimer and V-domain mixture in 1:2 molar ratio (1 V-domain per 1 S100B subunit). A complex of 54 kDa is formed and a residual peak of V-domain monomer is observed. The lower trace (–○–) shows S100B and V-domain mixture in 1:1 molar ratio. Clearly all V-domain is bound to S100B forming a complex of 36 kDa. (**B**) The upper trace (—) shows the analysis of V-domain. The middle trace (–▲–) shows S100B tetramer and V-domain mixture at 1:4 molar ratio (1 V-domain per 1 S100B subunit). A complex of 67 kDa and residual not bound V-domain is observed. The lower trace (–●–) shows S100B tetramer and V-domain mixture at 1:2 molar ratio. Again a complex of 67 kDa is observed. However, in contrast to the higher stoichiometries of V-domain per S100B tetramer almost no residual V-domain is observed.

Model of the RAGE V-domain and docking to S100B tetramer

It was reported previously that the N-terminal region of RAGE represents the ligand-binding site (Hofmann *et al*, 1999; Kislinger *et al*, 1999; Dattilo *et al*, 2007). To gain insights into a putative binding mode of S100B and a potential dimerisation of RAGE, a model of RAGE V-domain dimer was constructed (details for selection and evaluation of V-domain dimer model see 'Supplementary data'). *In silico* docking studies suggest that the S100B tetramer interacts with both V-domain molecules (Figure 8). In all docking solutions, one loop of one V-domain extends into the binding pocket formed by helices H_{III} and H_{IV} of S100B in the Ca^{2+}-loaded state. Such a binding mode is in agreement with the binding data, which show that only Ca^{2+}-loaded S100B can bind to sRAGE and with the data from analytical ultracentrifugation showing that one S100B tetramer binds two V-domain molecules. The residues involved in the contact between the V-domain model and S100B are well conserved in both molecules (Supplementary Figure III). A number of contacts are formed by residues from the loops of one V-domain with residues of helix H_{IV} and the hinge region of one S100B subunit. The second V-domain of the dimer forms contacts with two S100B subunits, mainly with the C terminus of helix H_{IV} of one subunit and helix H_{IV} and the canonical Ca^{2+}-binding loop of the second subunit.

Discussion

In this study, we show that S100B occurs in a multimeric state in human brain. Notably, the most prominent form is a

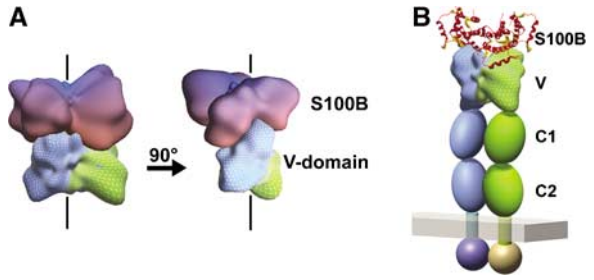

Figure 8 Model for RAGE dimerisation by tetrameric S100B. (**A**) Surface complementarity of S100B tetramer and V-domain dimer model. S100B tetramer and V-domain dimeric model are shown with harmonic spherical surfaces as calculated by Hex. The V-domain dimer model is coloured according to the chain identity (cyan and green) and S100B tetramer is coloured according to its distance to V-domain dimer; red corresponds to short and blue to long distances. (**B**) Schematic model of RAGE dimerisation. The RAGE molecules are coloured in green and cyan. The C-type Ig domains are depicted as ellipsoids and the intracellular domains as spheres. Bound S100B tetramer is shown as ribbon on top of the V-domain dimer model.

tetramer. Such noncovalent multimeric species were also detected on high-yield expression of human S100B in *E. coli* by us as well as independently by Sara Linse and co-workers (S Linse (Lund University, Sweden), personal communication; Linse and Thulin, submitted to Protein Science). However, such noncovalent multimers were not observed in previous NMR structural studies on S100B (Drohat *et al*, 1996, 1998b; Rustandi *et al*, 2000; Inman *et al*, 2002; Bhattacharya *et al*, 2003) by Weber and co-workers or Chazin and co-workers. We compared the protein purification protocols of both groups (Amburgey *et al*, 1995; Chazin, 2005) with our protocol. A striking difference in the preparation of S100B is the method of cell breakage. Whereas we use French press treatment throughout, the Weber and the Chazin group use ultrasonic disruption to break up the *E. coli* cells. Therefore, we tested whether conditions like during ultrasonic treatment could lead to disruption of tetrameric S100B. Before and after the treatment, the protein was analysed by analytical SEC. Clearly, the analysis shows that the S100B tetramer was disrupted into dimers by ultrasonic treatment (Supplementary Figure VII).

The isolated S100B multimers showed identical secondary structure content and Ca^{2+}-dependent conformational changes like the well-characterised S100B dimer. Obviously, the multimers are fully functional in signalling and do not represent aggregated or partially unfolded proteins.

Multimeric species of S100 proteins play a major role in extracellular and intracellular signalling. Very recently, it was shown that only a multimeric form of S100A4 has neurite sprouting activity (Kiryushko *et al*, 2006). Furthermore, a Ca^{2+}-induced S100A8/A9 tetramer (Korndörfer *et al*, 2007) promotes the formation of microtubules (Leukert *et al*, 2006) and additionally bound Ca^{2+} ions trigger the formation of a S100A12 hexamer, which interacts with RAGE (Xie *et al*, 2007). It was also reported previously (Koppal *et al*, 2001) that a disulphide-linked S100B molecule is active as neurite growth factor, whereas the S100B without disulphides can induce an inflammatory response in glia cells (Koppal *et al*, 2001). However, these studies on the extracellular activity of S100B did not clarify the quaternary structure of S100B. Here, we provide evidence that the noncovalent tetramers of S100B are highly stable and provide a structural clue for the stabilisation of such multimers.

The crystal structure of human S100B revealed an octameric organisation whereby four dimers form a tight assembly. This octamer assembles differently than the S100A8/A9 tetramer or the S100A12 hexamer (Moroz *et al*, 2002). In the S100A12 hexamer and in the S100A8/A9 tetramer, there are mainly polar interactions between the dimers, whereas in S100B, there are also hydrophobic residues contributing to the assembling. The key interacting residues for the S100B tetramer assembly reside on helix H_I and helix H_{IV}, which barely move upon Ca^{2+}-binding. In full agreement with the X-ray structural analysis, S100B tetramer in solution is stable in the Ca^{2+}-free form as observed by SEC or analytical ultracentrifugation (Figure 1). In contrast, S100A12 assembly to the hexamer or S100A8/A9 assembly to the tetramer is only possible in the Ca^{2+}-loaded state. In S100A12, the interdimer bridging Ca^{2+} ions are coordinated by residues residing in the C-terminal EF-hand and in helix H_{III} from two dimers. This arrangement of ligands for the interdimer Ca^{2+} coordination in S100A12 is only possible if the C-terminal EF-hand is already in the Ca^{2+}-loaded state. Similarly, Ca^{2+} loading of S100A8/A9 heterodimer is a prerequisite for tetramer formation. The pair of heterodimers displays a number of interactions comprising residues from the Ca^{2+}-loaded EF-hands of each S100A8 subunit, as well as residues from helix H_{IV} of each S100A9 subunit. Thus, the assembly of the S100A8/A9 tetramer and S100A12 hexamer are strictly dependent on Ca^{2+}, whereas the S100B tetramer is stable in the absence of Ca^{2+}. However, Ca^{2+} facilitated the assembly to hexamers and octamers as documented by SEC (Figure 1B) and by the additional Ca^{2+} ions observed at the proposed tetramer–tetramer interface (Figure 5). In summary, there is no general type of assembly in S100 protein multimers. A common feature in the multimeric structures of S100B and S100A12 are Ca^{2+} ions bound in addition to those in the EF-hands. These additional Ca^{2+} ions are located at the interface of the subunits and stabilise the larger aggregates. This finding implies that high Ca^{2+} concentrations will be required for the formation of the S100 protein multimers. Note that Ca^{2+} is present in millimolar concentrations in the extracellular space where S100A8/A9, S100A12 and S100B act as pro-inflammatory signalling molecules via the receptor RAGE.

In this study, we have analysed the binding of S100B to RAGE in real-time by SPR. We demonstrated that the interaction of S100B with RAGE is strictly Ca^{2+}-dependent. This finding was not expected, as the cytokine-like function of S100B might have been accomplished by structural features distinct from the Ca^{2+}-binding EF-hands. Moreover, tetrameric S100B dissociates from RAGE at a lower rate compared to the dimer resulting in high-affinity binding.

In a recent study (Dattilo *et al*, 2007), we analysed binding of S100B dimer to isolated domains of RAGE and observed significantly higher affinity binding of S100B dimer to V-domain and V-C1-domains than to entire sRAGE in this study. However, the domains in the study by Dattilo *et al* (2007) were covalently immobilised on the sensor chip. Apparently, the type of immobilisation influences the observed affinities. In view of the nanomolar to micromolar range of action reported for S100B (Huttunen *et al*, 2000), it is

not yet clear whether one study overestimated or underestimated the binding to RAGE.

The multiple binding sites of tetrameric S100B for RAGE will possibly trigger a multimerisation of the receptor, which has been established as a general mechanism for the initiation of signal transduction. Many cell-surface receptors are activated by a ligand-induced multimerisation process, such as Toll-like receptors (Hu *et al*, 2004; de Bouteiller *et al*, 2005) or the receptor for tumour necrosis factor α (Bazzoni *et al*, 1995). The role of the larger assemblies like hexamer and octamer of S100B remains still unclear and will be addressed in future research.

RAGE activation by S100B represents the major pro-inflammatory pathway in acute and chronic inflammatory diseases (Hofmann *et al*, 1999; Yan *et al*, 2003). Our structural and biochemical data provide insights into the mechanisms of S100B-induced RAGE multimerisation. The proposed binding mode derived from molecular modelling and docking calculations reveals highly complementary surfaces for tetrameric S100B and a RAGE V-domain dimer. These results represent a basis for ongoing studies on the entire ligand–receptor complex and on new approaches to intervene the S100–RAGE inflammatory axis.

Materials and methods

Expression and purification of proteins

Purification, crystallisation and X-ray analysis of recombinant S100B. Human S100B was purified and crystallised as described previously (Ostendorp *et al*, 2006) (see also Supplementary data).

Cloning, expression and purification of GST–sRAGE. The cDNA coding for containing the extracellular domain of human RAGE, sRAGE, (aa 23–322), was cloned via *Nde*I and *Xho*I into pHGST.2T vector, which was kindly provided by Dr S Meloche (University of Montreal, Canada). Transformed *E. coli* BL21(DE3) Origami B cells were grown to an optical density of 1.0 and induced with 1 mM IPTG. After overnight incubation at 30°C, the cells were harvested and resuspended in PBS containing protease inhibitors (Complete protease inhibitors; Roche Diagnostics). The cells were sonicated and the cytoplasmic extract was collected after centrifugation for 30 min at 20 000 *g*. The cytoplasmic extract was loaded onto a glutathione-Sepharose 4B column (GE-Healthcare) equilibrated with PBS. After 10 column volumes washing, the GST–sRAGE was eluted with 10 mM glutathione (Sigma). The concentration of the eluted protein was determined by the Bradford assay (Bio-Rad).

Purification of V-domain of human RAGE. Vector pET15b containing cDNA of V-domain of human RAGE (aa23–132) was kindly provided by Dr. B Dattilo (Vanderbilt University). The V-domain was purified as described elsewhere (Dattilo *et al*, 2007).

Analysis of S100B from human brain. Human postmortem brain sample was provided by Dr M Prinz, University of Göttingen and was in accordance with the recommendations of the ethics committee. The subject had no history of neurological disease nor had it indications of brain abnormalities at the tissue level as determined at autopsy. The brain sample from frontal lobe was frozen and stored at −70°C. All procedures were performed on ice. A 32 g portion of frozen human brain was thawed on ice and 15 ml of 50 mM Tris–HCl (pH 8.0) containing protease inhibitors (complete protease inhibitors, Roche Diagnostics) was added. The tissue was treated with a steel homogeniser and divided into three samples of 15 ml. One sample was stored at −70°C. The other samples were homogenised in buffer containing 20 mM DTT with either 10 mM EDTA or 20 mM $CaCl_2$ using a Potter–Elvehjem homogenizer. Brain extract was centrifuged for 1 h at 100 000 *g* at 4°C. Each supernatant was passed through a 0.2 μm filter and concentrated by ultrafiltration to a final volume of 0.7 ml. The two samples were loaded onto a Superdex 75 (1.6 × 60 cm) column (GE-Healthcare) equilibrated in 20 mM Tris–HCl, 150 mM NaCl (pH 7.6) containing either 1 mM EDTA or 4 mM $CaCl_2$. S100B concentration in the fractions was quantitated with the LIAISON Sangtec 100 assay (AB Sangtec Medical). Each determination was performed in triplicate according to the manufacturer's instructions.

Analytical methods

Size-exclusion chromatography. Analytical SEC was performed at room temperature on Superdex 75 (1.6 × 60 cm) and Superdex 75 (1.0 × 30 cm) columns connected to an AEKTA purifier system (GE-Healthcare). The different S100B multimers were separated at 4°C on a Superdex 75 (2.6 × 60 cm) column after reduction with an excess of DTT (100 mM). Running buffers for analytical SEC was 20 mM Tris–Cl, 150 mM NaCl (pH 7.6) and PBS for preparative SEC. Cytochrome *c* (12.4 kDa, Sigma), carboanhydrase (29 kDa, Sigma) and conalbumin (76 kDa, Serva) served as standards.

Analytical ultracentrifugation. Sedimentation velocity experiments for S100B were performed at 4°C in a Beckman ProteomeLab XL-I analytical ultracentrifuge with an An-50 Ti analytical rotor (Beckman) at a speed of 40 000 r.p.m. All data acquired from this experiment were obtained using the UV/Vis absorbance detection system on the ultracentrifuge at 280 or 245 nm and double sector 12 mm charcoal-filled Epon centrepieces. To monitor the interaction of dimeric and tetrameric S100B with V-domain of RAGE, the proteins were mixed in different ratios. These experiments were performed at 28°C. Protein concentration was 0.8–3 mg ml^{-1} in PBS or TBS containing 2 mM $CaCl_2$. Analysis of the continuous sedimentation coefficient distribution was performed with the software Sedfit v. 0.93 (Schuck, 2000) using the Lamm equation.

Cell culture and assay for cell proliferation and caspase 3 and 7 activities

The cervical carcinoma cell line HeLa was obtained from the European Collection of Animal Cell Cultures. Cells were grown at 37°C in Eagle's minimal essential medium (EMEM) supplemented with 10% (v/v) fetal bovine serum 1% penicillin and streptomycin and 2 mM glutamine in a humidified incubator with 5% carbon dioxide.

HeLa cells were seeded in 96-well culture plates (1.5×10^3 cells in 0.1 ml of EMEM/well) grown for 24 h in EMEM supplemented with 10% fetal bovine serum. At 12 h before incubation with or without S100B species, cells were starved in EMEM medium supplemented with 1% fetal bovine serum. Cell proliferation was quantified by absorbance at 595 nm using a Cell Proliferation Kit I (Roche) according to the manufacturer's instructions. Caspase 3 and 7 activities were measured with the same experimental conditions using the Caspase-Glo 3/7 Assay (Promega). All data are expressed as means ± s.d. Statistical analysis was performed using one-way analysis of variance, followed by Student's *t*-test. Significance was considered as $P \leqslant 0.0001$ (**) or $P \leqslant 0.001$ (*) versus the control group.

Surface plasmon resonance experiments

Immobilisation of GST antibody to CM5 sensor chips. Antibody against GST was purchased from Biacore International SA and was immobilised to CM5 sensor chip according to the manufacturer (Biacore). After immobilisation of anti-GST, the binding of GST (Biacore) was tested as a positive control. The flow rate was set to 50 μl/min and GST–sRAGE (75 μg/ml) was injected over the flow cell to be captured by the GST antibody, corresponding to an increase of about 1000 RU. Series of various concentrations from 0.5 to 10 μM of dimeric or tetrameric S100B in 50 mM Tris–HCl, 150 mM NaCl, 0.005% P2O (pH 7.4) containing either 2 mM $CaCl_2$ or 1 mM EDTA, were injected over the flow-cells. After each injection, the surface was regenerated with 50 mM glycine (pH 2.2).

Analysis of the sensorgrams. The binding curves were analysed by global analysis using BiaEvaluation 3.1 software (Biacore), which allows simultaneous fitting of association and dissociation of the different S100B concentrations (Roden and Myszka, 1996).

Structure determination and refinement

The structure of human S100B was solved by molecular replacement. The search model used for initial phase calculation was the structure of bovine S100B (PDB entry 1MHO). Rotation and

translation function analysis was performed using CNS (Brünger *et al*, 1998), including data from 15 to 4 Å resolution. Manual rebuilding of the model was done with the program O (Jones *et al*, 1991) and the model as refined to 1.90 Å resolution using refmac5 (Murshudov *et al*, 1997) from the CCP4 package (1994). Crystallographic data statistics are summarised in Table I.

Coordinates

The coordinates and structure factors have been deposited into the Protein Data Bank (PDB code 2H61).

Molecular modelling und docking studies

A 3D-model of the V-domain was built using MODELLER (Sali *et al*, 1995; Fiser and Sali, 2003). Model structures of the V-domain dimers were built using the dimeric T-cell receptor (1HBU) or Fab fragment (1MJU) as template for the spatial arrangement of two V-domains. The structural stability of the models generated from the different trials was tested by means of molecular dynamics simulations. Docking calculations of tetrameric S100B with the final V-domain dimer model were performed using Hex 4.5 (Ritchie and Kemp, 2000; Mustard and Ritchie, 2005) (for details of molecular modelling and docking studies see Supplementary data).

Supplementary data

Supplementary data are available at *The EMBO Journal* Online (http://www.embojournal.org).

Acknowledgements

We thank Dr Wolfram Welte for providing the X-ray facilities at the University of Konstanz, Dr Kay Diederichs and Dr Andre Schiefner (University of Konstanz, Germany) for helpful discussions, Dr Brian Dattilo and Dr Walter J Chazin (Vanderbilt University, USA) for preparing the Cys→Ser mutant of S100B and Dr Christophe Briand (University of Zurich, Switzerland) for performing analytical ultracentrifugation runs. We gratefully acknowledge the support of the SLS PX beamline at the Paul Scherrer Institute (Villigen, Switzerland). This work was supported by the TR-SFB (DFG), the Swiss National Science Foundation (Grant No. 3100A0-10970) and the Wilhelm Sander-Stiftung.

References

Amburgey JC, Abildgaard F, Starich MR, Shah S, Hilt DC, Weber DJ (1995) 1H, 13C and 15N NMR assignments and solution secondary structure of rat Apo-S100β. *J Biomol NMR* **6:** 171–179

Bazzoni F, Alejos E, Beutler B (1995) Chimeric tumor necrosis factor receptors with constitutive signaling activity. *Proc Natl Acad Sci USA* **92:** 5376–5380

Bhattacharya S, Large E, Heizmann CW, Hemmings B, Chazin WJ (2003) Structure of the Ca^{2+}/S100B/NDR kinase peptide complex: insights into S100 target specificity and activation of the kinase. *Biochemistry* **42:** 14416–14426

Brünger AT, Adams PD, Clore GM, DeLano WL, Gros P, Grosse-Kunstleve RW, Jiang JS, Kuszewski J, Nilges M, Pannu NS, Read RJ, Rice LM, Simonson T, Warren GL (1998) Crystallography & NMR system: a new software suite for macromolecular structure determination. *Acta Crystallogr D Biol Crystallogr* **54:** 905–921

Businaro R, Leone S, Fabrizi C, Sorci G, Donato R, Lauro GM, Fumagalli L (2006) S100B protects LAN-5 neuroblastoma cells against Abeta amyloid-induced neurotoxicity via RAGE engagement at low doses but increases Abeta amyloid neurotoxicity at high doses. *J Neurosci Res* **83:** 897–906

CCP4 (1994) The CCP4 suite: programs for protein crystallography. *Acta Crystallogr D* **50:** 760–763

Chazin WJ (2005) http://structbio.vanderbilt.edu/chazin/wisdom/labpro/S100B_purification.html

Dattilo BM, Fritz G, Leclerc E, Vander Kooi CW, Heizmann CW, Chazin WJ (2007) The extracellular region of the receptor for advanced glycation end products is comprised of two independent structural units. *Biochemistry* **46:** 6957–6970

Davey GE, Murmann P, Heizmann CW (2001) Intracellular Ca^{2+} and Zn^{2+} levels regulate the alternative cell density-dependent secretion of S100B in human glioblastoma cells. *J Biol Chem* **276:** 30819–30826

de Bouteiller O, Merck E, Hasan UA, Hubac S, Benguigui B, Trinchieri G, Bates EE, Caux C (2005) Recognition of double-stranded RNA by human toll-like receptor 3 and downstream receptor signaling requires multimerization and an acidic pH. *J Biol Chem* **280:** 38133–38145

Donato R (2003) Intracellular and extracellular roles of S100 proteins. *Microsc Res Tech* **60:** 540–551

Drohat AC, Amburgey JC, Abildgaard F, Starich MR, Baldisseri D, Weber DJ (1996) Solution structure of rat apo-S100B(beta beta) as determined by NMR spectroscopy. *Biochemistry* **35:** 11577–11588

Drohat AC, Baldisseri DM, Rustandi RR, Weber DJ (1998a) Solution structure of calcium-bound rat S100B (ββ) as determined by nuclear magnetic resonance spectroscopy. *Biochemistry* **37:** 2729–2740

Drohat AC, Baldisseri DM, Rustandi RR, Weber DJ (1998b) Solution structure of calcium-bound rat S100B(betabeta) as determined by nuclear magnetic resonance spectroscopy. *Biochemistry* **37:** 2729–2740

Drohat AC, Tjandra N, Baldisseri DM, Weber DJ (1999) The use of dipolar couplings for determining the solution structure of rat apo-S100B(betabeta). *Protein Sci* **8:** 800–809

Fiser A, Sali A (2003) ModLoop: automated modeling of loops in protein structures. *Bioinformatics* **19:** 2500–2501

Freigang J, Proba K, Leder L, Diederichs K, Sonderegger P, Welte W (2000) The crystal structure of the ligand binding module of axonin-1/TAG-1 suggests a zipper mechanism for neural cell adhesion. *Cell* **101:** 425–433

Griffin WS, Sheng JG, McKenzie JE, Royston MC, Gentleman SM, Brumback RA, Cork LC, Del Bigio MR, Roberts GW, Mrak RE (1998) Life-long overexpression of S100β in Down's syndrome: implications for Alzheimer pathogenesis. *Neurobiol Aging* **19:** 401–405

Heizmann CW, Fritz G, Schäfer BW (2002) S100 proteins: structure, functions and pathology. *Front Biosci* **7:** d1356–d1368

Hofmann MA, Drury S, Fu C, Qu W, Taguchi A, Lu Y, Avila C, Kambham N, Bierhaus A, Nawroth P, Neurath MF, Slattery T, Beach D, McClary J, Nagashima M, Morser J, Stern D, Schmidt AM (1999) RAGE mediates a novel proinflammatory axis: a central cell surface receptor for S100/calgranulin polypeptides. *Cell* **97:** 889–901

Hu X, Yagi Y, Tanji T, Zhou S, Ip YT (2004) Multimerization and interaction of Toll and Spatzle in *Drosophila*. *Proc Natl Acad Sci USA* **101:** 9369–9374

Huttunen HJ, Kuja-Panula J, Sorci G, Agneletti AL, Donato R, Rauvala H (2000) Coregulation of neurite outgrowth and cell survival by amphoterin and S100 proteins through receptor for advanced glycation end products (RAGE) activation. *J Biol Chem* **275:** 40096–40105

Ikura M, Ames JB (2006) Genetic polymorphism and protein conformational plasticity in the calmodulin superfamily: two ways to promote multifunctionality. *Proc Natl Acad Sci USA* **103:** 1159–1164

Inman KG, Yang R, Rustandi RR, Miller KE, Baldisseri DM, Weber DJ (2002) Solution NMR structure of S100B bound to the high-affinity target peptide TRTK-12. *J Mol Biol* **324:** 1003–1014

Jones TA, Zou JY, Cowan SW, Kjeldgaard M (1991) Improved methods for building protein models in electron density maps and the location of errors in these models. *Acta Crystallogr A* **47:** 110–119

Kabsch W, Sander C (1983) Dictionary of protein secondary structure: pattern recognition of hydrogen-bonded and geometrical features. *Biopolymers* **22:** 2577–2637

Kilby PM, Van Eldik LJ, Roberts GC (1996) The solution structure of the bovine S100B protein dimer in the calcium-free state. *Structure* **4:** 1041–1052

Kiryushko D, Novitskaya V, Soroka V, Klingelhofer J, Lukanidin E, Berezin V, Bock E (2006) Molecular mechanisms of Ca^{2+} signaling in neurons induced by the S100A4 protein. *Mol Cell Biol* **26:** 3625–3638

Kislinger T, Fu C, Huber B, Qu W, Taguchi A, Du Yan S, Hofmann M, Yan SF, Pischetsrieder M, Stern D, Schmidt AM (1999) N(epsilon)-(carboxymethyl)lysine adducts of proteins are ligands for receptor for advanced glycation end products that activate cell signaling pathways and modulate gene expression. *J Biol Chem* **274:** 31740–31749

Koppal T, Lam AG, Guo L, Van Eldik LJ (2001) S100B proteins that lack one or both cysteine residues can induce inflammatory responses in astrocytes and microglia. *Neurochem Int* **39:** 401–407

Korndörfer IP, Brueckner F, Skerra A (2007) The crystal structure of the human $(S100A8/S100A9)_2$ Heterotetramer, Calprotectin, illustrates how conformational changes of interacting alpha-helices can determine specific association of two EF-hand proteins. *J Mol Biol* **370:** 887–898

Lawrence MC, Colman PM (1993) Shape complementarity at protein/protein interfaces. *J Mol Biol* **234:** 946–950

Leukert N, Vogl T, Strupat K, Reichelt R, Sorg C, Roth J (2006) Calcium-dependent tetramer formation of S100A8 and S100A9 is essential for biological activity. *J Mol Biol* **359:** 961–972

Lo Conte L, Chothia C, Janin J (1999) The atomic structure of protein–protein recognition sites. *J Mol Biol* **285:** 2177–2198

Marenholz I, Heizmann CW, Fritz G (2004) S100 proteins in mouse and man: from evolution to function and pathology (including an update of the nomenclature). *Biochem Biophys Res Commun* **322:** 1111–1122

Matsumura H, Shiba T, Inoue T, Harada S, Kai Y (1998) A novel mode of target recognition suggested by the 2.0 Å structure of holo S100B from bovine brain. *Structure* **6:** 233–241

McClintock KA, Shaw GS (2003) A novel S100 target conformation is revealed by the solution structure of the Ca^{2+}-S100B-TRTK-12 complex. *J Biol Chem* **278:** 6251–6257

Moroz OV, Antson AA, Dodson EJ, Burrell HJ, Grist SJ, Lloyd RM, Maitland NJ, Dodson GG, Wilson KS, Lukanidin E, Bronstein IB (2002) The structure of S100A12 in a hexameric form and its proposed role in receptor signalling. *Acta Crystallogr D* **58:** 407–413

Mrak RE, Griffin WS (2001) The role of activated astrocytes and of the neurotrophic cytokine S100B in the pathogenesis of Alzheimer's disease. *Neurobiol Aging* **22:** 915–922

Murshudov GN, Vagin AA, Dodson EJ (1997) Refinement of Macromolecular Structures by the Maximum-Likelihood Method. *Acta Crystallogr D* **53:** 240–255

Mustard D, Ritchie DW (2005) Docking essential dynamics eigenstructures. *Proteins* **60:** 269–274

Nayal M, Di Cera E (1996) Valence screening of water in protein crystals reveals potential Na^+ binding sites. *J Mol Biol* **256:** 228–234

Neeper M, Schmidt AM, Brett J, Yan SD, Wang F, Pan YC, Elliston K, Stern D, Shaw A (1992) Cloning and expression of a cell surface receptor for advanced glycosylation end products of proteins. *J Biol Chem* **267:** 14998–15004

Nishiyama H, Knöpfel T, Endo S, Itohara S (2002) Glial protein S100B modulates long-term neuronal synaptic plasticity. *Proc Natl Acad Sci USA* **99:** 4037–4042

Ostendorp T, Heizmann CW, Kroneck PMH, Fritz G (2005) Purification, crystallization and preliminary X-ray diffraction studies on human Ca^{2+}-binding protein S100B. *Acta Crystallograph Sect F Struct Biol Cryst Commun* **61:** 673–675

Ostendorp T, Weibel M, Leclerc E, Kleinert P, Heizmann CW, Kroneck PMH, Fritz G (2006) Expression and purification of the soluble isoform of human receptor for advanced glycation end products (sRAGE) from *Pichia pastoris*. *Biochem Biophys Res Commun* **347:** 4–11

Ramasamy R, Vannucci SJ, Yan SS, Herold K, Yan SF, Schmidt AM (2005) Advanced glycation end products and RAGE: a common thread in aging, diabetes, neurodegeneration, and inflammation. *Glycobiology* **15:** 16R–28R

Ritchie DW, Kemp GJ (2000) Protein docking using spherical polar Fourier correlations. *Proteins* **39:** 178–194

Roden LD, Myszka DG (1996) Global analysis of a macromolecular interaction measured on BIAcore. *Biochem Biophys Res Commun* **225:** 1073–1077

Rustandi RR, Baldisseri DM, Weber DJ (2000) Structure of the negative regulatory domain of p53 bound to S100B(ββ). *Nat Struct Biol* **7:** 570–574

Sali A, Potterton L, Yuan F, van Vlijmen H, Karplus M (1995) Evaluation of comparative protein modeling by MODELLER. *Proteins* **23:** 318–326

Schuck P (2000) Size-distribution analysis of macromolecules by sedimentation velocity ultracentrifugation and lamm equation modeling. *Biophys J* **78:** 1606–1619

Selinfreund RH, Barger SW, Pledger WJ, Van Eldik LJ (1991) Neurotrophic protein S100 beta stimulates glial cell proliferation. *Proc Natl Acad Sci USA* **88:** 3554–3558

Soroka V, Kolkova K, Kastrup JS, Diederichs K, Breed J, Kiselyov VV, Poulsen FM, Larsen IK, Welte W, Berezin V, Bock E, Kasper C (2003) Structure and interactions of NCAM Ig1-2-3 suggest a novel zipper mechanism for homophilic adhesion. *Structure* **11:** 1291–1301

Xie J, Burz DS, He W, Bronstein IB, Lednev I, Shekhtman A (2007) Hexameric Calgranulin C (S100A12) binds to the receptor for advanced Glycated end products (RAGE) using symmetric Hydrophobic target-binding patches. *J Biol Chem* **282:** 4218–4231

Yan SS, Wu ZY, Zhang HP, Furtado G, Chen X, Yan SF, Schmidt AM, Brown C, Stern A, LaFaille J, Chess L, Stern DM, Jiang H (2003) Suppression of experimental autoimmune encephalomyelitis by selective blockade of encephalitogenic T-cell infiltration of the central nervous system. *Nat Med* **9:** 287–293

